Geophysical Research Letters

Supporting information for

The stratospheric pathway for Arctic impacts on mid-latitude climate

Tetsu Nakamura[1,2*], Koji Yamazaki[1,2], Katsushi Iwamoto[3], Meiji Honda[4], Yasunobu Miyoshi[5], Yasunobu Ogawa[6,7], Yoshihiro Tomikawa[6,7], and Jinro Ukita[4]

[1] Arctic Environmental Research Center, National Institute of Polar Research, Tokyo 190-8518, Japan

[2] Faculty of Environmental Earth Science, Hokkaido University, Hokkaido 060-0810, Japan

[3] Mombetsu city government, Hokkaido 094-8707, Japan

[4] Department of Environmental Science, Niigata University, Niigata 950-2181, Japan

[5] Department of Earth and Planetary Sciences, Kyushu University, Fukuoka 812-8581, Japan

[6] Space and Upper Atmospheric Sciences Group, National Institute of Polar Research, Tokyo 190-8518, Japan

[7] SOKENDAI (The Graduate University for Advanced Studies), Tokyo 190-8518, Japan

[*] Corresponding author: T. Nakamura (nakamura.tetsu@ees.hokudai.ac.jp)

Contents of this file

Text S1 to S5

Figures S1 to S5

S1. Restoring force and resultant changes in zonal mean zonal wind variability

Vertical profiles of the relaxation coefficient of restoring force applied in *RS10* and *RS30* are shown in Fig. S1a. The coefficient was linearly interpolated between the lowest and higher levels (Methods in the text). As a result of this relaxation, internal variability of the zonal mean zonal wind at 60°N for January greatly decreased in the stratosphere (Fig. S1b). Stratospheric variations did not vanish in the stratosphere restoration experiments because the restoring force (maximum value 1 d^{-1}) was weak compared with the wave drag due to the internal variation of the planetary wave. From those we see that the spread among the experiments in the stratosphere is larger for the monthly time scale variability than for the daily time scale variability. The restoration results in reduction in internal variability at monthly time scale as intended. In contrast, shorter time scale variability is less affected by the restoration.

S2. Biases in the restoring stratosphere (RS) experiments

To examine possible influences of the artificial restoring force on mean circulation, we compared the climatologies of the zonal mean zonal wind and EP flux and its divergence among *HICE* runs of the three experiments. First the model simulated winter climatologies of the zonal mean zonal wind (contours in Fig. S2a) were reasonably close to the observation (not shown). With respect to *FREE*, the *RS10* and *RS30* experiments showed negative anomalies ("biases" in color) in the strength of the polar night jet (colors in Fig. S2a). Propagation characteristics of wave activity indicated by the EP flux (green arrows in Fig. S2b) were similar among the experiments, but the vertical component in the stratosphere were slightly larger in the *RS10* and *RS30* experiments. As a result, climatological EP flux convergence became stronger in the mid- to upper-stratosphere (broken lines in Fig. S2b). It is possible to explain this by a balance between the restoring force and internal wave forcing in the restored stratosphere. Planetary wave continuously propagated upward while the polar vortex breakdown occurred less frequently due to the restoration.

There is another possibility that a weaker zonal wind bias in the lower stratosphere might have changed the sensitivity for the wave propagation and thus affected the resultant polar vortex fluctuation (Smith et al., 2010; Nishii et al., 2011; Kim et al., 2014). However, the lower stratospheric wave activity responses to the sea ice changes in *RS10* and *RS30* were weaker than in *FREE* (Fig. 2b). And the biases in the wave activity for *RS10* and *RS30* were positive, i.e. stronger upward propagation into the stratosphere (Fig. S2b). From those, it is likely that the bias on the resultant anomalies due to the sea ice change were small.

S3. Nature of the planetary-scale wave in the lower stratosphere

The climatological distribution of eddy geopotential height (i.e., departure from its zonal mean) clearly showed a wave-2 structure in January at 100 hPa (Fig. S3a). The trough and ridge amplitude was largest over Siberia and Alaska. The corresponding wave activity flux was then obtained on the basis of the three-dimensional EP flux [*Plumb,* 1985]. Because the three-dimensional EP flux was calculated using monthly mean data, the resulting wave activity fluxes indicate propagation of the quasi-stationary wave. Upward wave propagation into the upper stratosphere was seen over the Eurasian-Pacific sector, and its maximum was located in eastern Siberia (120–150°E, 60°N) (Fig. S3b). This result is reasonable because baroclinicity is strong there, where an upper level trough sits over the surface Siberian high in winter.

S4. Persistence in upward propagation of the wave activity

Fz anomalies significantly differed between *FREE* and the restored experiments (Fig. 2c). The magnitudes of Fz anomalies were similar in all three cases, but only in *FREE* the anomaly was sustained with stronger persistence, which is favorable to disturb the upper stratospheric polar vortex. It is unclear whether the artificial restoring forcing directly reduces the persistence level in the upward propagation of the wave activity or the wave activity dynamically interacts with the stratospheric conditions themselves. To address this question we examined how persistent the wave activity was in terms of lag structure for all three cases.

Here we argue that the lead-lag correlation coefficients between Fz at 100 hPa and other levels represent how persistent the wave activity behaves (Fig. S4a). There were no differences among three experiments, indicating that the restoring forcing did not

alter the persistence in the wave activity. In contrast, responded height anomalies due to the wave drag showed changed behaviour in the persistence in the stratosphere (Fig. S4b), i.e. stronger in *FREE* compared with the *RS* cases. Those results suggest that the longer duration (stronger persistence) in the wave activity results from dynamical interactions between the mean state of the stratosphere and the wave activity in the lower stratosphere. We then interpret different *LICE*-minus-*HICE* anomalies among the three experiments as follows: (*FREE* case) The anomalous wave activity due to the sea ice changes disturbed the upper stratosphere and the resultant changes in the stratosphere affected back to the wave activity to be more persistent. (*RS* cases) The upper stratosphere did not respond to the wave drag from the restoration. Then the anomalous wave activity did not persist because of a lack of changes in the stratospheric conditions.

S5. Sea-ice impacts on the autumn snow cover in the Eurasia

Changes in autumn snow cover due to the sea-ice reduction were estimated as the *LICE*-minus-*HICE* anomaly of the snow cover extent. Small patchy anomalies indicated less snow cover along the Arctic coast of central Siberia and more snow cover in eastern Siberia (Fig. S5a). The total of the snow anomaly over the Siberian region seem to be near zero, suggesting that, at least in our model, sea ice had no impact on the autumn snow cover.

We also examined the simulated relationship between autumn snow cover and winter AO. Simulated AO is defined as the EOF1 of geopotential height anomalies at 500 hPa (Z500) northward of 30°N. EOF was calculated with DJF-averaged Z500 anomalies of 120 years (*HICE*+*LICE*) of the *FREE* experiment. The AO time series (AOI) is defined as the EOF1 score. The October snow cover extent (SCE) is defined as the year-to-year time series of SCE in October averaged over the Siberian region (67.5°–141.0°E, 36.5°–68.0°N, surrounded by the green line in Fig. S3a). October SCE negatively correlated with AO phase in the following DJF (Fig. S5b). This snow–AO relationship is consistent with earlier reports [*Fletcher et al.,* 2007; *Liu et al.,* 2012]. However, because sea ice had no impact on the autumn snow cover (Fig. S5a), the negative AO signal of the *LICE*-minus-*HICE* anomaly simulated in *FREE* was mostly due to the sea-ice reduction, independent of the autumn snow cover.

References

Fletcher, C. G., P. J. Kushner & J. Cohen, Stratospheric control of the extratropical circulation response to surface forcing. *Geophys. Res. Lett.* **34,** L21802 (2007).

Kim, B. M., S. W. Son, S. K. Min, J. H. Jeong, S. J. Kim, Z. Zhang, T. Shim, & J. H. Yoon, Weakening of the stratospheric polar vortex by Arctic sea-ice loss. *Nature Communications* **5**, 4646 (2014).

Liu, J. P., J. A. Curry, H. Wang, M. Song & R. M. Horton, Impact of declining Arctic sea ice on winter snowfall. *Proc. Natl. Acad. Sci.* **109,** 4074–4079 (2012).

Nishii, K., H. Nakamura & Y. J. Orsolini, Geographical dependence observed in blocking high influence on the stratospheric variability through enhancement or suppression of upward planetary-wave propagation. *J. Clim.* **24**, 6408–6423 (2011).

Plumb, R. A. On the Three-Dimensional Propagation of Stationary Waves. *J. Clim.* **42,** 217–229 (1985).

Smith, K. L., C. G. Fletcher, & P. J. Kushner, The role of linear interference in the Annular Mode response to extratropical surface forcing. *J. Clim.* **23**, 6036–6050 (2010).

Figures

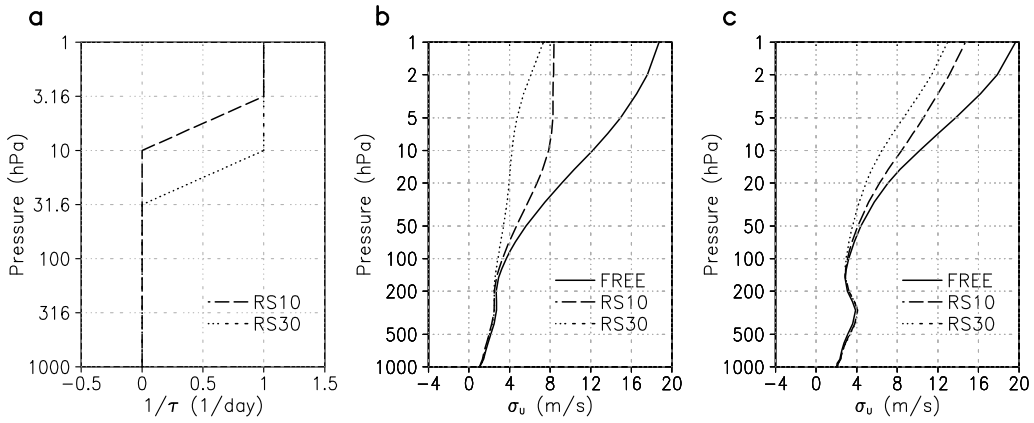

Figure S1. a, Vertical profiles of relaxation forcing applied in the *RS10* and *RS30* experiments. **b,** Standard deviations of the interannual variations of the monthly mean zonal mean zonal wind at 60°N in January in the *FREE*, *RS10*, and *RS30* experiments, obtained from the 60-year output of the *HICE* runs. **c,** Same as **b** but for mean standard deviations of daily departure from the monthly mean.

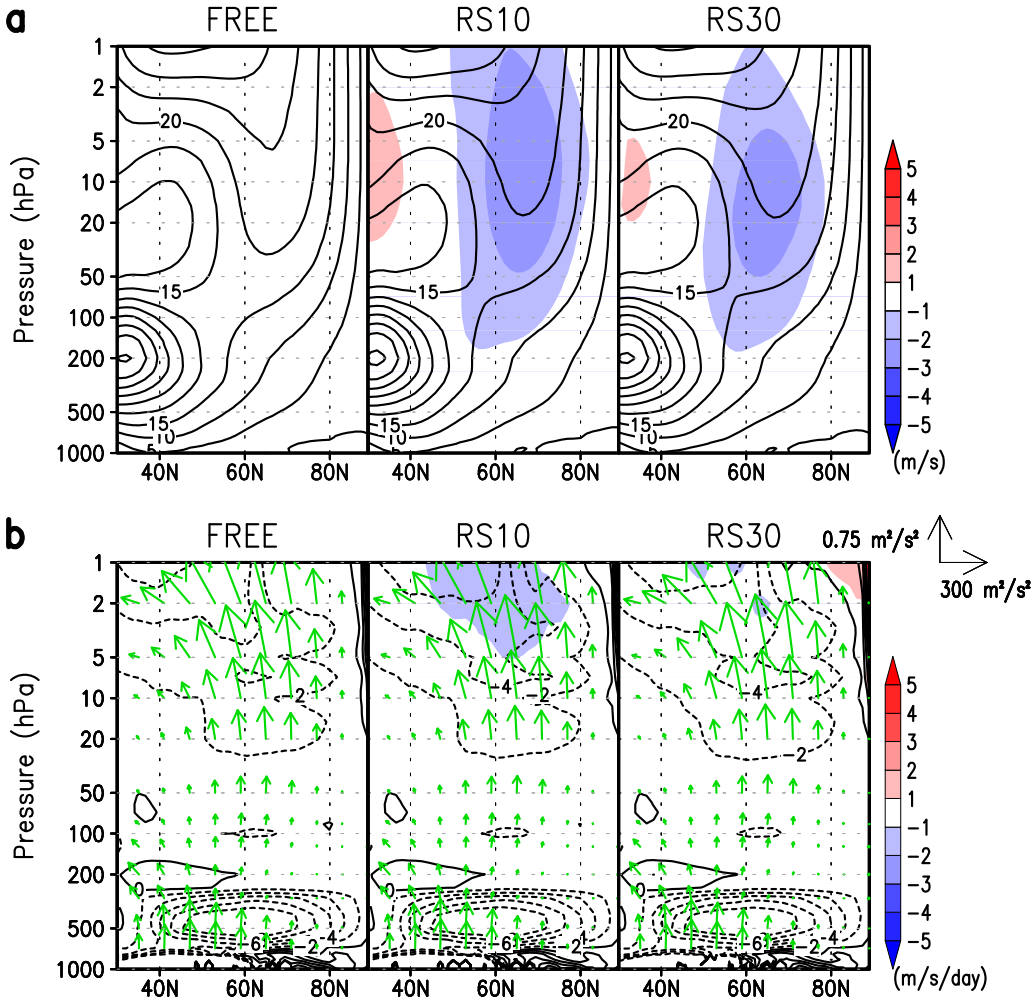

Figure S2. a, Latitude-height cross sections of 60-year climatologies of the DJF averaged zonal mean zonal wind of *HICE* run in the individual experiments. Corresponding experimental name is designated at the top of the panel. Contours indicate the climatologies and colors indicate departures of relaxation experiments from *FREE* experiment. **b,** As in **a** but for EP flux divergence. Arrows indicate EP flux vectors. Magnitude of flux was standardized by p/p_s and Earth's radius. Arrow length corresponding to 300 $m^2\ s^{-2}$ for meridional component and 0.75 $m^2\ s^{-2}$ for vertical component is designated at top-right of the figure.

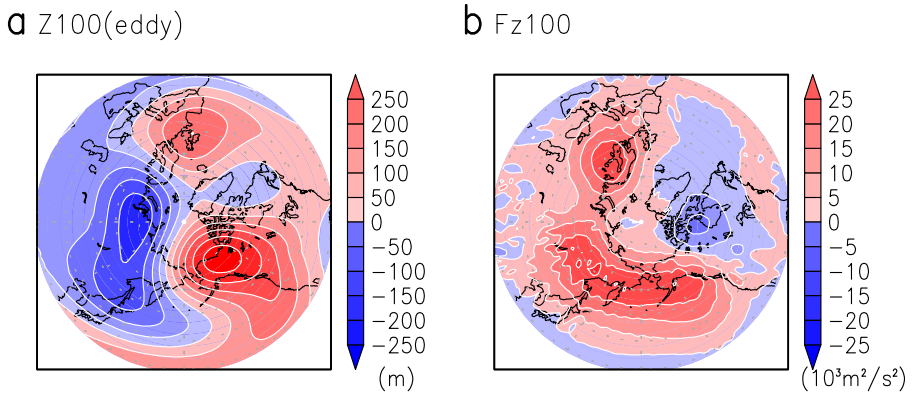

Figure S3. January climatology of **a,** eddy geopotential height (i.e., departure from its zonal mean) (m) and **b,** vertical component of wave activity flux (10^3 m^2 s^{-2}). Climatology here means the 60-year average in the *HICE* run of *FREE*.

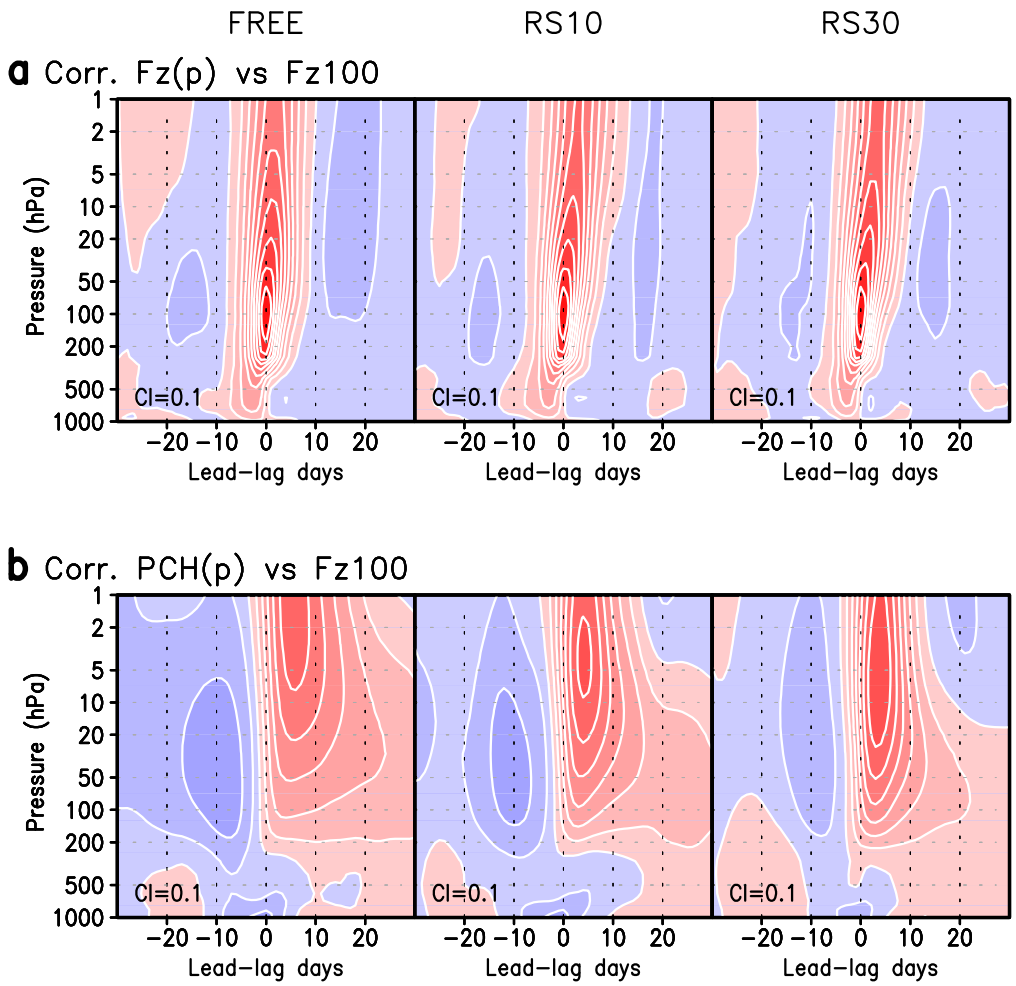

Figure S4. a, Lead-lag correlation coefficients of 50-80N averaged vertical component of the EP flux (Fz) at various pressure levels with Fz at 100 hPa during the 90 days of winter (December, January, and February) of *HICE* run. Red (blue) shading indicates positive (negative) correlations; contour interval is 0.1. **b,** Same as **a** but for correlation of polar cap height (PCH) at various pressure levels with Fz at 100 hPa.

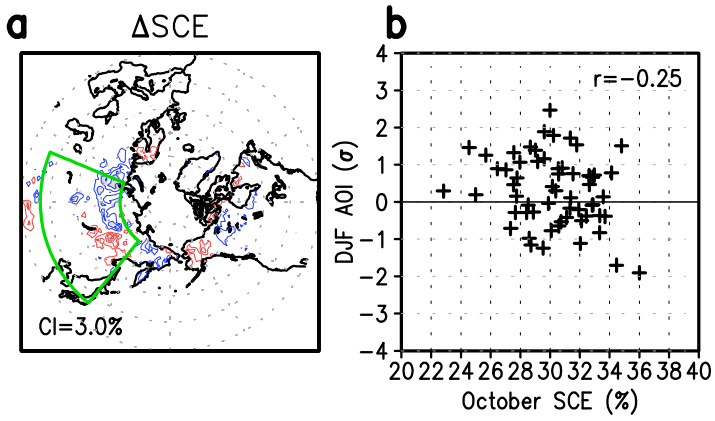

Figure S5. a, *LICE*-minus-*HICE* anomaly of snow cover extent (ΔSCE) in October in *FREE*. Contour interval is 3.0%, and the zero line is omitted. Red and blue indicate positive and negative values, respectively. Light and heavy grey shadings indicate a statistical significance greater than 95% and 99%, respectively. **b,** Scatter diagram plotting the October SCE time series versus the DJF AOI in the *HICE* run in *FREE*. The October SCE time series was defined as snow cover extent averaged over the Siberian area (67.5–141.0°E, 36.5–68.0°N; surrounded by the green line in **a**).